Hemispheric asymmetry of entrained auditory steady state responses arise from the structural connectome

Authors: Neeraj Kumar, Amit Kumar Jaiswal, Dipanjan Roy, Arpan Banerjee*

Cognitive Brain Dynamics Lab, National Brain Research Centre, NH 8, Manesar, Gurgaon, 122052, India.

Email: arpan@nbrc.ac.in

Abstract: Structure-function relationships are of fundamental importance to biological systems. In the human auditory system, it has been demonstrated that asymmetric neuroanatomic embedding of primary auditory cortices in the whole brain network is predictive of functional lateralisation. However, a mechanistic and causal basis of the functional asymmetry due to the underlying structural constraints is poorly understood. The present article takes the help of computational modelling to demonstrate how functional lateralization emerges from the symmetries in structural connectome. First, we demonstrate a well-known lateralisation effect observed during entrainment of external rhythmic auditory stimulus at the level of cortical sources from EEG data. Subsequently, we simulate the dynamics of whole brain cortical responses from large-scale neurodynamic model using realistic connection topologies. Considering the effects of time-delay stemming from physical fibre distances computed from diffusion imaging metrics, and neuronal scaling and coupling based on empirical data, we could elucidate the biophysically realistic parameter regimes where the structural connectome is predictive of functional lateralisation. Thus our study provides a roadmap in causally linking structural symmetries to higher order brain function.

1. Introduction:

Several studies suggest that both structural and functional networks are asymmetrically distributed in the brain (Semmes, 1968; R J Zatorre & Belin, 2001) where each hemisphere is optimised to perform specialised tasks (Toga & Thompson, 2003). A popular example of functional asymmetry is dichotomous lateralisation in the processing auditory objects. For instance, speech and language are predominantly processed in the left hemisphere while right hemisphere is specialised for processing of music or rhythmic stimuli (Ross, Herdman, & Pantev, 2005; R J Zatorre & Belin, 2001). Asymmetry in the brain is thought to reflect evolutionary, developmental, experiential and pathological factors. However, mechanisms, origin or reasons behind this functional asymmetry is not resolved yet.

From an anatomical perspective there are asymmetric structural efferent projections from the auditory cortex in each hemisphere (Andoh, Matsushita, & Zatorre, 2015). This may contribute to the emergence of hemispheric specialization during processing of distinct features of auditory stimuli (Cammoun et al., 2015; Robert J Zatorre & Gandour, 2008). More recently, applying network analysis tools on diffusion-weighted imaging data Mišić and colleagues showed that the both auditory cortices are asymmetrically integrated in the whole brain structural network and this may result in the lateralized auditory responses (Mišić et al., 2018). Consequently, if there is asymmetry in the afferent anatomical input to the auditory cortex; one can hypothesize that hemispheric dominance should also depend on the ear of stimulation. Thus, an identical stimulus may elicit asymmetrically lateralized responses for monaural left and right stimulations. Study of such asymmetric responses not only helps in deciphering functional organization of the auditory system but also has clinical applications for studying experience-related changes in the case of

unilateral hearing impairment (Hine & Debener, 2007) or age related hearing impairments (Henry, Herrmann, Kunke, & Obleser, 2017). However, a key question that is still poorly understood is whether there is any causal link between large-scale structure of the brain and functional hemispheric specialisation.

Among functional responses that are of cortical origin, auditory steady state rhythms (ASSR) elicited by a periodic tonal stimulation has been identified as a potential marker of auditory processing (Mendel, 1980; Lins & Picton, 1995; Picton, John, Dimitrijevic, & Purcell, 2003). There are strong evidences that neural generators for ASSRs predominantly lie in primary auditory cortex (Gutschalk et al., 1999; Ross et al., 2005)) and distributed auditory areas (Farahani, Goossens, Wouters, & van Wieringen, 2017; Coffey et al., 2016), with activity more pronounced in the right hemisphere. Nonetheless, the generators of ASSRs are embedded in a whole-brain network displaying wide range of complex brain dynamics. Till date the mechanisms of this dynamical entrainment is out of scope of any study.

Emerging evidence suggests that biophysical models of the whole-brain that embeds the realistic structural constraints can reveal the mechanisms underlying functional responses (Ghosh, Rho, McIntosh, Kötter, & Jirsa, 2008; Honey, Kötter, Breakspear, & Sporns, 2007, Suarez et al 2020). In the present study, we use a large-scale neurodynamic model to identify the generative mechanisms of functional asymmetry of ASSRs. In particular, we have asked whether constraints in whole-brain structural connectivity with auditory brain regions as seed, is the cause of the asymmetry in brain functional organization. To address this, we collected empirical EEG

data using a tonal (1kHz) auditory stimulus repeated at 40 Hz to generate ASSRs during binaural, monaural left and monaural right conditions. We characterized the asymmetric functional organization of cortical responses at the sensor and source level power at 40 Hz. Subsequently, using the Kuramoto phase oscillators placed at locations guided by diffusion tensor imaging data (Abeysuriya et al 2018) and coupled via distance scaling from fibre densities we could generate simulated ASSRs that retains the empirical symmetry. The mechanisms of ASSRs generation was evaluated from comparisons between empirical and simulated data.

89 # 2. Materials and Methods

90 ## 2.1 Participants

91 Twenty-one healthy, right-handed human volunteers (16 males, 5 females, age range 22-39 years
92 old; mean ± SD = 28 ± 2.10) participated in this study[1]. All the volunteers reported no medical
93 history of audiological, neurological or psychiatric disorders. All of them had normal or
94 corrected to normal visual acuity. Informed consents were given by all the volunteers in a format
95 approved by the Institutional Human Ethics Committee (IHEC) of National Brain Research
96 Centre. All participants were fluent in at least two languages, Hindi and English, but some were
97 familiar more languages of Indian origin. All volunteers were undergraduate degree holders.
98

99 ## 2.2 Experimental design

100 Stimuli consisted of sinusoidal tones of 1 KHz frequency with 5% rise and fall, presented 40
101 times per second (Linden, Picton, Hamel, & Campbell, 1987). Each trial comprised of 1s "On"
102 block (auditory stimulation) period followed by 1s "Off" block (silent) period (Figure 1A). A
103 total of 100 trials ("On" blocks) were presented for each kind of auditory stimulation, monaural
104 and binaural. In total, four experimental conditions, each lasting 200 seconds were performed in
105 the following order: 1) a baseline condition in which the volunteers were not given any tonal
106 stimuli; 2) Binaural (in both ears); 3) Monaural left (only through left ear); 4) Monaural right
107 (only through right ear) (Figure 1B). The time interval between each condition was set to 100 s
108 (silent). Auditory stimuli were created and presented in Stim2 software (Compumedics, Inc.,

[1] A subset of this data (10 volunteers) were used in a Methods paper Halder, T; Talwar, S., Jaiswal, A.K., Banerjee, A.(2019): Quantitative evaluation in estimating sources underlying brain oscillations using current source density methods and beamformer approaches. eNeuro. 2019 Jul-Aug; 6(4): ENEURO.0170-19.2019.

USA) at the intensity of 90 dB. Participants were instructed to stay still in sitting position, fixate on a visual cross displayed on a computer screen for the duration, and listen to the tones. When the volunteers were performing the experiment, continuous scalp EEG was recorded with relevant trigger data.

2.3 Neuroimaging procedure

EEG data were recorded using 64 high-density Ag/AgCl sintered electrodes mounted in an elastic head cap according to the international 10-20 system. All recordings were done in a noise proof isolated room using NeuroScan (SynAmps2) system (Compumedics Inc, USA) with 1 KHz sampling rate. Abrasive electrolyte gel (EASYCAP) was used to make a contact between EEG sensors and scalp surface and impedance was maintained at values less than 5 kΩ in each sensor throughout the entire experiment. The EEG system-assigned reference electrode at the vertex was selected for reference and the forehead (AFz) electrode as the ground.

2.4 Pre-processing of EEG signals

EEG data were imported in MATLAB using EEGLAB from Neuroscan raw files. Epochs of 1000 ms from "On" blocks were extracted from each trial. The resulting epochs were then bandpass filtered to retain frequencies in the range 2 to 48 Hz, followed by detrending (baseline correction) of data to remove any linear trends from the signal. Trials having a voltage greater than ±100 μv were considered as artifacts and therefore discarded. All trials from both monaural conditions of participant 15 were full of artefacts; therefore we had removed data of participant 15 for further analysis. Furthermore, since the objective was to estimate the steady-state activity of the brain, we concatenated time series of ten consecutive epochs (while keeping their temporal

order intact) to enhance spectral resolution. Trials from all participants were grouped together, resulting in a time series of 10s for each condition.

2.5 Spectral analysis

Multi-tapered power spectral density was computed using Chronux function *mtspectrumc.m* (http://chronux.org/) and customized MATLAB (www.mathworks.com) scripts at each sensor, trial and condition. Power spectra of the concatenated time series were calculated in the frequency range of 2 - 48 Hz having a frequency resolution of 0.06 Hz with time-bandwidth product and number of tapers set at 5 and 3, respectively, as the input parameters. Subsequently, differences in spectral power at 40 Hz (frequency of interest) between auditory stimulation tasks and baseline condition were statistically evaluated by means of a permutation test using ft_freqstatistics.m, a function of fieldtrip toolbox (www.fieldtriptoolbox.org). Paired-sample t-statistic between auditory stimulation and baseline condition was computed at each sensor. Additionally, to circumvent multiple comparison problem we clustered sensors based on their spatial adjacency (Maris, Schoffelen, & Fries, 2007). Therefore, neighboring electrodes having t-value higher than $t_{185} = 3.63$ or lower than $t_{185} = -4.01$; $p < 0.05$ were counted as a cluster. Afterwards, cluster statistics were derived by taking the sum of t - statistics across a cluster which was compared with the null distribution of cluster statistics generated by random permutation procedure (1000 times). Subsequently, the statistical significance of the spectral difference between the two conditions was assessed by using a two-tailed t-test in which the observed test statistic value of the cluster was the threshold at 95^{th} percentile of the null distribution. *p*-values of the clusters were obtained by estimating the proportion of clusters from the null distribution that are beyond the aforesaid threshold.

2.6 Source reconstruction

We performed exact low-resolution brain electromagnetic tomography (eLORETA) (Pascual-Marqui, 2007) to locate the stimulus-specific sources of 40 Hz ASSRs. First, as a head model, we used the standardized boundary element method (BEM) volume conduction model of the human head as a common template for all participants (Oostenveld, Stegeman, Praamstra, & van Oosterom, 2003). We discretized the brain volume into 2807 regularly spaced three-dimensional cubic. The centre of the cubic grid had the coordinates following the Montreal Neurological Institute (MNI) template. Furthermore, employing the sensors location information along with the head model we created a leadfield for each grid.

Subsequently, to obtain the oscillatory sources of 40 Hz activity we employ distributed source modelling using exact low-resolution brain electromagnetic tomography (eLORETA). eLORETA estimates the current source density across brain volume by minimizing the surface Laplacian component during the construction of the spatial filter (Pascual-Marqui, 2007, Pascual-Marqui, et al., 2011). Additionally, eLORETA does not rely upon any assumption regarding the number of underlying sources while having a very good control over suppression of false positives during detection of sources (Halder, Talwar, Jaiswal, & Banerjee, 2019). The source analysis was performed using Fieldtrip toolbox (Oostenveld, Fries, Maris, & Schoffelen, 2011; http://fieldtriptoolbox.org). The ingredients to construct a frequency domain eLORETA filter are the forward model and the cross-spectral matrix of sensor data. Hence, we computed sensor-level cross-spectral matrix from 'On' blocks time series (i.e., 1 s) after re-referencing the EEG data on common average reference for all conditions. Thereafter, a common spatial filter was computed employing combined data from all conditions. A common filter attenuates filter specific variability during inverse modelling i.e., the observed difference between different

conditions is attributed only to the differences in conditions not due to differences in the spatial filter. Spatial filter for each grid was then calculated in 3 orthogonal directions. Since we do not have any prior assumption about the orientation of the underlying source, therefore, the cross-spectra of sensor data were projected through the strongest orientation of dipole i.e., denoting maximum variance. Consequently, a 3D distribution of source power across brain volume was obtained. Afterwards, prominent sources were selected after thresholding the source power distribution at 95th quantile. Supra-thresholded sources were visualized by rendering onto the Colin27 brain template.

2.7 Neurodynamic model

We obtained structural connectivity and fiber length matrices from an online dataset derived from diffusion MRI probabilistic tractography of 40 participants (Abeysuriya et al., 2018). Obtained structural connectivity matrix was parcellated in 68 regions according to the Desikan–Killiany brain atlas. Subsequently, we simulated a network of 68 coupled Kuramoto oscillators, each oscillator representative of a brain parcel. The oscillators were coupled according to empirically derived anatomical strengths and time delays. Each hemisphere constituted an equal set of 34 nodes. SC matrix and fiber length matrix both were symmetric matrices representing mean white matter densities and distance among nodes, respectively. Coupling strength matrix was normalized between 0 and 1 such that the maximum strength among connections was 1. The values at the diagonals of the connection strength and fiber length matrix representing self-connectivity and length with self, respectively, were set at zero (see Supplementary Material).

To imbibe the realism of primary generators of ASSRs lie in auditory cortex, we chose two nodes in the primary auditory cortex (PAC) (and other 66 nodes in rest of brain as non-auditory nodes (non-PAC). Using the Kuramoto model (Kuramoto et al., 1984) the phase dynamics of any non-PAC nodes is defined as

$$\dot{\theta_n} = \omega_n + k\sum_{p=1}^{N} C_{np} sin\left(\theta_p\left(t-\tau_{np}\right) - \theta_n(t)\right), \forall n = 1,2 \dots N-2 \quad (1)$$

where ω_n represents the intrinsic frequency of the oscillator as $\omega_n = 2\pi f_n$; k is mean coupling strength used to scale the all coupling strengths; τ represents mean transmission delay employed to calculate time step delays among nodes given the length of the fiber. In equation (1) the value of p iterates from 1 to 68 including auditory nodes. This implies that phase dynamics of non-PAC will depend on phase dynamics of all other nodes including both auditory nodes. However, phase dynamics of the PAC nodes are defined as,

$$\dot{\theta_A} = \omega_A \quad , \qquad \text{where} \quad \omega_A = 2\pi * f_A$$

After setting frequency of non-PAC nodes (f_n) at 10 Hz and frequency of PAC (f_A) nodes at 40 Hz, we investigated hemispheric laterality indices across a model parameter space, wherein k values range from 1 to 50 and τ values from 4 to 12. τ values in this range correspond to the bio-physiologically realistic communication speed of around 5-20 m/s in adult primate brain (Ghosh et al., 2008). For every τ value employing fiber length matrix we estimated the time delays matrix that are involved in transmitting information between any pair of nodes (Cabral, Hugues, Sporns, & Deco, 2011). Similarly, structural connectivity was transformed into the coupling strength matrix$C$. These transformations imply that coupling strength and delay

between any pair of nodes will be proportional to the structural connectivity and fiber length matrix. Hence, C_{np} and τ_{np} respectively represents the coupling strength and time delay between node n and$p$. Therefore, the dynamics of theta at any node will be a function of its anatomical strength and distance with other nodes. The model was simulated for about 25 seconds. We took sine of theta obtained at each node which represents a simulation of neural time series at EEG source level. Subsequently, we calculated the power spectral density from 68 nodes followed by hemispheric laterality analysis of the spectral power at 40 Hz (See more in section 2.8). During monaural condition simulations we asymmetrically scaled the relative coupling strengths of both PAC nodes with non-PAC nodes by the ratio of spectral power we obtained empirically between left and right hemisphere auditory parcels after source reconstruction. Remaining procedure remained same as described above for binaural condition simulation.

2.8 Laterality analysis

Hemispheric asymmetry in brain responses was quantified using laterality indices (*LI*), which is the difference between right hemisphere (RH) and left hemispheric (LH) responses normalized by the sum of response in both hemispheres.

$$LI = \frac{RH-LH}{RH+LH} \quad (6)$$

Value of *LI* lies between +1 and -1. Wherein +1 represent complete right hemispheric dominance, -1 for complete left hemispheric dominance and 0 for bilaterally symmetric response. *LI*s for spectral power were computed at source level for empirical and theoretical dataset.

3. Results

3.1 Spectral topography of ASSRs

Grand mean power spectra (and subject-wise power spectra [see Figure S1]) averaged over all electrodes and volunteers showed enhancement of spectral power specifically at 40 Hz (Figure 2A) in both monaural and binaural conditions relative to the silent baseline. Differences between the topographic scalp distribution at 40 Hz during auditory stimulations and the baseline were evaluated using cluster-based permutation tests (See Methods). Significant enhancement of spectral power at 40 Hz in distributed scalp sensor locations was observed (Figure 2B). The purple "*" on the topoplots in Figure 2B maps the position of electrodes that are significantly different from the baseline condition at 95% confidence level. Overall, the pattern of distribution of enhancement in the spectral power at 40 Hz was found to be similar in both binaural and monaural conditions. However, differences in magnitudes were observed across different conditions and both hemispheres. In summary, we have observed two significant clusters of spectral power during every stimulation condition. Wherein one large cluster was located over the fronto-central area and another in bi-lateral caudal parts of the scalp (Figure 2 B and Table 1). However, the channels in the right posterior region showed greater enhancement compared to their counterpart in left hemisphere during binaural and monaural right condition. As a sanity check, we further validated the presence of right hemispheric dominance during binaural condition in different temporal segments (early, middle and late ERP components) of "On" block.

3.2 Source-level functional organisation of 40 Hz ASSRs

We used exact low-resolution brain electromagnetic tomography (eLORETA) to calculate the three-dimensional spatial distribution of source activity and identified the prominent sources of 40 Hz ASSRs. Reconstructed sources were rendered onto a standard cortical surface derived from colin27 brain provided in fieldtrip toolbox (http://fieldtriptoolbox.org). The locations of prominent sources during monaural left, monaural right and binaural condition are shown in Figure 3. Anatomical labels (According to Desikan-Killiany atlas) corresponding to source regions and number of activated voxels in the respective region are summarised in Table 2. We found distributed sources of 40 Hz ASSRs in auditory cortices and beyond auditory cortices. We found main activations in the temporal lobe (bilateral STG, MTG and ITG), supramarginal, inferior frontal gyrus, bilateral pre-central gyrus, bilateral post-central gyrus, and occipital lobe. Majority of the sources exhibited right hemisphere dominance irrespective of the stimulation condition. Activation in right transverse temporal is unique during monaural left condition. Left MTG showed significant activation only during monaural left and binaural condition but not during the monaural right condition. Laterality indices (LI) computed from source power revealed right hemispheric dominance during the every type of stimulation condition. Particularly, during binaural condition (mean LI = 0.09), monaural left condition (mean LI = 0.10 and during monaural right condition (mean LI = 0.20).

3.3 Neural Dynamical Model

We modelled each parcellated brain area (using Desikan Killiany atlas), as Kuramoto phase oscillator, coupled by coupling coefficients and time delay that were derived from empirical diffusion tensor imaging data (see Methods for details, Figure 4A). The nodes in auditory cortex

were driven by 40 Hz external inputs while keeping the intrinsic frequency of other nodes at 10 Hz. The system of differential equations were numerically integrated using Euler integration method for 250000 time points with a step size (dt) of 0.0001. The initial 10000 time points were removed before power spectral density was computed from remaining 15000 time points representing source time series of 15 seconds duration, at a sampling rate of 1000 Hz. Thereafter, we calculated the hemispheric laterality indices (LI) from spectral power distribution at 40 Hz. Figure 4C demonstrates the LI values across a range of k (1 to 50) and τ (4 to 12) values. Positive LI values were obtained across all over parameter space spanned by k and τ. In particular the LI value ranged (0.02, 0.07] for monaural left condition, (0.03, 0.08] for monaural right condition and (0.01, 0.058] for binaural condition. However, we also found that LI varies as a function of both time delay and mean coupling strength. Specifically, for every type of simulation condition LI increased positively (Right hemispheric dominance) when coupling (k) and speed of transmission (τ) increases. The topology of LI across (k, τ) space during all conditions were similar. Finally, we compared the LI obtained from the model with the empirical LI in Figure 4B. For that purpose, we selected the values of k (k = 230) and τ ($\tau = 4$) that yielded the maximum match with empirical LI values after simulation of model with parameter k ranging from 1 to 300, while keeping tau fixed at 4. The resulting mean LI values for each condition are bin: 0.07, monaural left: 0.09, monaural right: 0.11.

4. Discussion

ASSRs involve synchronization of distributed neuronal assemblies to a periodic external input (Pastor et al., 2002; Reyes et al., 2005). Heschl's gyri situated in primary auditory cortices are known to be the first cortical structure to receive auditory information. Subsequently, information from primary auditory cortices is segregated to the specialised higher order cortical structures to resolve and process features of auditory stimuli. Misic and colleagues suggested that there is asymmetry in communication pathways among both primary auditory cortices to other brain regions may contribute to functional lateralisation in auditory system (Mišić et al., 2018). In the present study we demonstrated the role of whole-brain structural connectome in which the auditory brain regions are embedded in guiding the hemispheric functional asymmetry of ASSR. First, we replicated the earlier findings of entrained 40 Hz oscillations representing amplitude modulation of the auditory stimuli corroborating previous studies (Galambos, Makeig, & Talmachoff, 1981; Hari et al., 1989; Linden et al., 1987). The enhanced auditory steady state response (ASSRs) was dominant over the right hemisphere which replicates earlier studies (Ross et al., 2005). Second, we localise sources of sensor level 40 Hz activity wherein temporal gyri being a major player of asymmetry during 40 Hz ASSRs. Third, by simulating auditory nodes as externally driven oscillators in a whole-brain network of Kuramoto oscillators we could accurately predict the functional lateralization of ASSR. Importantly, regardless of the fact that the SC matrices were not of the participants from whom the EEG data was collected the combination of computational model and structural connectivity still could explain the functional asymmetry, in a wide range of biologically realistic time-delays and coupling.

Sources beyond the auditory cortex

We used eLORETA to locate sources of 40 Hz ASSRs during binaural and both monaural conditions, as it has been proved, specifically for 40 Hz ASSRs in a subset of dataset used here, to show significant control over the false positive ratio in the distributed dipole condition (Halder et al., 2019). In addition to classic auditory pathway, we also report strongest activation beyond primary auditory cortex as well. For instance, brain regions in inferior parietal gyrus, pre-central and post-central gyrus, inferior and middle frontal gyrus and occipital cortex (Table 2), which is in line with earlier findings on reconstructed 40 Hz ASSRs sources with equivalent dipole modelling. Farahani and colleagues identified distributed sources in both cortical and subcortical regions during 4, 20, 40, and 80 Hz ASSRs (Farahani, Goossens, Wouters, & van Wieringen, 2017). Our study reveals that right hemispheric dominance during binaural condition is not solely limited to core auditory areas but regions beyond primary auditory areas also contribute to right hemispheric lateralization (Table 2, Figure 3). During every type of stimulation condition, we found prominent sources among bilateral supra-temporal gyri, pre-central and post-central gyri. Activation in superior temporal gyrus (STG) is corroborated with earlier findings (Mäkelä & Hari, 1987). Core areas of auditory cortex are highly responsive to pure tones (tonotopic organization), surrounded by belt regions that are responsive to more complex tones (cochleotopic organization) (Banerjee, Kikuchi, Mishkin, Rauschecker, & Horwitz, 2018). We have found several 40 Hz oscillatory sources in spatially distinct brain regions, which are in general involved in different stages in the hierarchy of information processing during binaural and both monaural conditions. In a PET-weighted LORETA neuroimaging study Reyes and colleagues reported prominent activation in right temporal lobe and right parietal lobe along with activations in right frontal lobe during monaural right condition (Reyes et al., 2005). Several

studies have also reported anatomical projections from STG to frontal cortex (Hackett, 2011; Kaas & Hackett, 2000; Plakke & Romanski, 2014). Wang and colleagues identified functional network comprising of frontal cortex and superior temporal regions that are sensitive to tone repetition pattern, which is associated with human's unique ability for language processing (Wang, Uhrig, Jarraya, & Dehaene, 2015). Hence, our results supports the view that auditory processing at a very basic level requires other brain areas beyond primary auditory cortices.

Asymmetric lateralization of brain rhythms

A key finding of our study is the right hemispheric dominance revealed by the laterality analysis during the most environmentally realistic hearing condition of binaural stimulation. This is in line with the previous finding that suggested tonal or melodic stimuli are predominantly processed in the right hemisphere while speech and language stimuli showed left hemisphere dominance (Albouy et al., 2020; Ross et al., 2005; R J Zatorre & Belin, 2001). Ross and colleagues further proposed that right hemisphere dominance during ASSRs may be the result of processing temporal regularities associated with pitch processing of incoming sound (Ross et al., 2005). More recently, applying network analysis tools on diffusion tensor imaging data Misic and colleagues showed that the right auditory cortex is better integrated with other parts of the brain and this may result in the right hemispheric primacy to complex cognitive processing such as music (Mišić et al., 2018). Thus, the explanation of observed functional right hemispheric dominance may partly lie in the anatomical asymmetries of the structural connectome that embeds auditory cortical areas. A more explicit demonstration of this hypothesis came from our computational study. For the purpose of the current manuscript we undertook source-level analysis using eLORETA to get an distribution of 40 Hz ASSRs to understand if there are

particular brain regions that may have a contribution on functional asymmetry. Almost all the top sources showed right hemispheric dominance irrespective of the stimulation condition. The number of sources and their power in the right hemisphere was more than that of the left hemisphere during binaural stimulation, thus, following the same reverberating theme of right hemispheric dominance.

Another key finding of our study is that at source level right hemisphere was largely dominant during every stimulation condition. However, if we compare activations in hemisphere among conditions rather than their equivalent area in other hemisphere we found among monaural conditions left hemisphere was more dominant during monaural condition. Specifically, left middle temporal gyri are activated in monaural left condition but not during monaural right condition. Additionally, number of voxels in left lateral occipital lobe, STG, post-central gyrus, and fusiform were greater during monaural left condition than monaural right condition. This implies greater activation during ipsilateral ear stimulation compared to the contralateral ear stimulation. In an EEG study Reyes and colleagues (Reyes et al., 2005) reported ipsilateral dominance in temporal lobe /inferior parietal lobe (IPL) during 40 Hz -ASSRs. The dominance of ipsilateral (right) PoG and IPL during monaural right condition was also reported by Pastor and Reyes, respectively during 40 Hz ASSRs (Pastor et al., 2002; Reyes et al., 2005).

Characterizing hemispheric dominance in the functional specialization of sensory processing is a fundamental question in cognitive neuroscience. There are many factors that are posed as to influence lateralisation in brain including anatomical asymmetries, stimulus designs, sex and handedness of the participant (Hutsler & Galuske, 2003; Melynyte et al., 2017; Tervaniemi et al.,

2000). The main contribution of our study is the demonstration of how functional lateralization of ASSR, is an outcome of the dynamical evolution of spatiatemporal brain patterns via neural interactions scaffolded by the structural connectome. Structural connection is been known to play a role in determining functional connectivity (Honey et al., 2007). We propose that the structural connectome gives rise to two important physiological constraints, time-delays of propagation of information among brain areas, and possible neural covariates dependent on tissue properties such as white matter density, myelination that are also subject to neuroplasticity. This provides further opportunity to expand the model to tests different groups of volunteers, such as musicians whose auditory systems may have higher fidelity and across life span ageing where the tissue parameters of brain has changed. The validation of our model in such data sets will be certainly one of our main targets in future.

While our study lays out the 40 Hz ASSRs at the scalp and source level, however, there are certain limitations to the result that can be improved in the future. One immediate factor that can shape up the right-hemisphere dominance is the role of language. Although we did not test the participants on their linguistic or auditory processing skills, all our participants were self-declared bi-literates and in some cases knew more than two Indian languages. Second, we did not choose participants based on their musical training which can be a potential future direction to look for pattern differences. Third, an interesting extension for the asymmetrical differences we report can be explored in data sets present in the literature from neurodevelopmental disorders such as autism and neuropsychiatric disorders like schizophrenia. An important direction of ASSRs research is to define normative patterns of cortical auditory processing beyond the simple audiological tests. This is where we propose our results would be most

valuable and more focussed research delineating our patterns from neural disorders is needed in the future. If we can use some language like stimuli and see the emergence of asymmetry then we can prove that which features of speech or language (intelligibility or spectral / temporal cues) given the right hemispheric structural dominance dictate the asymmetry in the auditory system.

Conflict of Interest Statement

The authors declare no conflicts of interest.

Acknowledgments

The study was supported by NBRC Core funds and by grants Ramalingaswami fellowship, (BT/RLF/Re-entry/31/2011) and Innovative Young Bio-technologist Award (IYBA), (BT/07/IYBA/2013) from the Department of Biotechnology (DBT), Ministry of Science and Technology, Government of India to AB. DR was supported by the Ramalingaswami fellowship (BT/RLF/Re-entry/07/2014) from DBT and extramural grant SR/CSRI/21/2016/ from Department of Science and Technology (DST), Ministry of Science and Technology, Government of India. AB and DR are jointly supported by BT/MED-III/NBRC/Flagship/Program/2019 from DBT. We sincerely thank late Dr. Jeffrey Michael Valla for constructive comments on an earlier version of this manuscript and Dr. Subham Kumar for helpful discussions and suggestions.

References

Abeysuriya, R. G., Hadida, J., Sotiropoulos, S. N., Jbabdi, S., Becker, R., Hunt, B. A. E., Woolrich, M. W. (2018). A biophysical model of dynamic balancing of excitation and inhibition in fast oscillatory large-scale networks. *PLoS Computational Biology*, *14*(2). https://doi.org/10.1371/journal.pcbi.1006007

Albouy, P., Benjamin1, L., Morillon, B., & Zatorre, R. J. (2020). Distinct sensitivity to spectrotemporal modulation supports brain asymmetry for speech and melody. *Science*, *367*(6481), 1043–1047. https://doi.org/10.1126/science.aaz3468

Andoh, J., Matsushita, R., & Zatorre, R. J. (2015). Asymmetric Interhemispheric Transfer in the Auditory Network: Evidence from TMS, Resting-State fMRI, and Diffusion Imaging. *Journal of Neuroscience*, *35*(43), 14602–14611. https://doi.org/10.1523/JNEUROSCI.2333-15.2015

Banerjee, A., Kikuchi, Y., Mishkin, M., Rauschecker, J. P., & Horwitz, B. (2018). Chronometry on Spike-LFP Responses Reveals the Functional Neural Circuitry of Early Auditory Cortex Underlying Sound Processing and Discrimination. *Eneuro*, *5*(3), ENEURO.0420-17.2018. https://doi.org/10.1523/ENEURO.0420-17.2018

Cabral, J., Hugues, E., Sporns, O., & Deco, G. (2011). Role of local network oscillations in resting-state functional connectivity. *NeuroImage*, *57*(1), 130–139. https://doi.org/10.1016/j.neuroimage.2011.04.010

Cammoun, L., Thiran, J. P., Griffa, A., Meuli, R., Hagmann, P., & Clarke, S. (2015). Intrahemispheric cortico-cortical connections of the human auditory cortex. *Brain Structure and Function*, *220*(6), 3537–3553. https://doi.org/10.1007/s00429-014-0872-z

Coffey, E. B. J., Herholz, S. C., Chepesiuk, A. M. P., Baillet, S., & Zatorre, R. J. (2016). Cortical

contributions to the auditory frequency-following response revealed by MEG. Nature Communications, 7. https://doi.org/10.1038/ncomms11070

Farahani, E. D., Goossens, T., Wouters, J., & van Wieringen, A. (2017). Spatiotemporal reconstruction of auditory steady-state responses to acoustic amplitude modulations: Potential sources beyond the auditory pathway. *NeuroImage*, *148*, 240–253. https://doi.org/10.1016/j.neuroimage.2017.01.032

Galambos, R., Makeig, S., & Talmachoff, P. (1981). A 40-Hz auditory potential recorded from the human scalp. *Proceedings of the National Academy of Sciences of the United States of America*, *78*(4), 2643–2647. https://doi.org/10.1073/pnas.78.4.2643

Ghosh, A., Rho, Y., McIntosh, A. R., Kötter, R., & Jirsa, V. K. (2008). Noise during Rest Enables the Exploration of the Brain's Dynamic Repertoire. *PLoS Computational Biology*, *4*(10), e1000196. https://doi.org/10.1371/journal.pcbi.1000196

Gutschalk, A., Mase, R., Roth, R., Ille, N., Rupp, A., Hähnel, S., Scherg, M. (1999). Deconvolution of 40 Hz steady-state fields reveals two overlapping source activities of the human auditory cortex. *Clinical Neurophysiology*, *110*(5), 856–868. https://doi.org/10.1016/S1388-2457(99)00019-X

Hackett, T. A. (2011). Information flow in the auditory cortical network. *Hearing Research*, *271*(1–2), 133–146. https://doi.org/10.1016/j.heares.2010.01.011

Halder, T., Talwar, S., Jaiswal, A. K., & Banerjee, A. (2019). Quantitative evaluation in estimating sources underlying brain oscillations using current source density methods and beamformer approaches. *ENeuro*, *6*(4). https://doi.org/10.1523/ENEURO.0170-19.2019

Hari, R., Hämäläinen, M. S., & Joutsiniemi, S. L. (1989). Neuromagnetic steady-state responses to auditory stimuli. *J Acoust Soc Am*, *86*(3), 1033–1039. https://doi.org/10.1121/1.398093

Henry, M. J., Herrmann, B., Kunke, D., & Obleser, J. (2017). Aging affects the balance of neural entrainment and top-down neural modulation in the listening brain. *Nature Communications*, *8*(1), 15801. https://doi.org/10.1038/ncomms15801

Hine, J., & Debener, S. (2007). Late auditory evoked potentials asymmetry revisited. *Clinical Neurophysiology*, *118*(6), 1274–1285. https://doi.org/10.1016/j.clinph.2007.03.012

Honey, C. J., Kötter, R., Breakspear, M., & Sporns, O. (2007). Network structure of cerebral cortex shapes functional connectivity on multiple time scales. *Proceedings of the National Academy of Sciences of the United States of America*, *104*(24), 10240–10245. https://doi.org/10.1073/pnas.0701519104

Hutsler, J., & Galuske, R. A. W. (2003). Hemispheric asymmetries in cerebral cortical networks. *Trends in Neurosciences*. Trends Neurosci. https://doi.org/10.1016/S0166-2236(03)00198-X

Kaas, J. H., & Hackett, T. A. (2000). Subdivisions of auditory cortex and processing streams in primates. *Proceedings of the National Academy of Sciences*, *97*(22), 11793–11799. https://doi.org/10.1073/pnas.97.22.11793

Kuramoto, Y. (1984). Chemical Oscillations, Waves, and Turbulence (Vol. 19). Berlin, Heidelberg: Springer Berlin Heidelberg. https://doi.org/10.1007/978-3-642-69689-3

Linden, R. D., Picton, T. W., Hamel, G., & Campbell, K. B. (1987). Human auditory steady-state evoked potentials during selective attention. *Electroencephalography and Clinical Neurophysiology*, *66*(2), 145–159. https://doi.org/10.1016/0013-4694(87)90184-2

Lins, O. G., & Picton, T. W. (1995). Auditory steady-state responses to multiple simultaneous stimuli. *Electroencephalography and Clinical Neurophysiology/ Evoked Potentials*, *96*(5), 420–432. https://doi.org/10.1016/0168-5597(95)00048-W

514 Mäkelä, J. P., & Hari, R. (1987). Evidence for cortical origin of the 40-Hz auditory evoked
515 response in man. *Electroencephalography and Clinical Neurophysiology*, *66*, 539–546.
516 Maris, E., Schoffelen, J. M., & Fries, P. (2007). Nonparametric statistical testing of coherence
517 differences. *Journal of Neuroscience Methods*, *163*(1), 161–175.
518 https://doi.org/10.1016/j.jneumeth.2007.02.011
519 Melynyte, S., Pipinis, E., Genyte, V., Voicikas, A., Rihs, T., & Griskova-Bulanova, I. (2017). 40
520 Hz Auditory Steady-State Response: The Impact of Handedness and Gender. *Brain*
521 *Topography*, *31*(3), 419–429. https://doi.org/10.1007/s10548-017-0611-x
522 Mendel, M. I. (1980). Clinical use of primary cortical responses. *Audiology*, *19*(1), 1–15.
523 Retrieved from http://www.ncbi.nlm.nih.gov/pubmed/6986148
524 Mišić, B., Betzel, R. F., Griffa, A., Reus, M. A. De, He, Y., Zuo, X., Zatorre, R. J. (2018).
525 Network-based asymmetry of the human auditory system. *Cerebral Cortex*, (May), 1–14.
526 https://doi.org/10.1093/cercor/bhy101
527 Oostenveld, R., Fries, P., Maris, E., & Schoffelen, J.-M. (2011). FieldTrip: Open source software
528 for advanced analysis of MEG, EEG, and invasive electrophysiological data. *Computational*
529 *Intelligence and Neuroscience*, *2011*, 156869. https://doi.org/10.1155/2011/156869
530 Oostenveld, R., Stegeman, D. F., Praamstra, P., & van Oosterom, A. (2003). Brain symmetry and
531 topographic analysis of lateralized event-related potentials. *Clinical Neurophysiology :*
532 *Official Journal of the International Federation of Clinical Neurophysiology*, *114*(7), 1194–
533 1202. Retrieved from http://www.ncbi.nlm.nih.gov/pubmed/12842715
534 Pantev, C., Roberts, L. E., Elbert, T., Ross, B., & Wienbruch, C. (1996). Tonotopic organization
535 of the sources of human auditory steady-state responses. *Hear Res*, *101*(1–2), 62–74.
536 https://doi.org/10.1016/S0378-5955(96)00133-5

Pascual-Marqui, R. D. (2007). Discrete, 3D distributed, linear imaging methods of electric neuronal activity. Part 1: exact, zero error localization. Retrieved from http://arxiv.org/abs/0710.3341.

Pascual-Marqui, R. D., Lehmann, D., Koukkou, M., Kochi, K., Anderer, P., Saletu, B., Tanaka, H., Hirata, K., John, E. R., Prichep, L., Biscay-Lirio, R. and Kinoshita, T. (2011) Assessing interactions in the brain with exact low-resolution electromagnetic tomography. *Philos Trans A Math Phys Eng Sci*, 369(1952), pp. 3768-84.

Pastor, M. A., Artieda, J., Arbizu, J., Marti-Climent, J. M., Peñuelas, I., & Masdeu, J. C. (2002). Activation of human cerebral and cerebellar cortex by auditory stimulation at 40 Hz. *The Journal of Neuroscience : The Official Journal of the Society for Neuroscience*, *22*(23), 10501–10506. Retrieved from http://www.ncbi.nlm.nih.gov/pubmed/12451150

Picton, T. W., John, M. S., Dimitrijevic, A., & Purcell, D. (2003). Human auditory steady-state responses. *International Journal of Audiology*, *42*(4), 177–219. https://doi.org/10.1182/blood-2016-09-739086

Plakke, B., & Romanski, L. M. (2014). Auditory connections and functions of prefrontal cortex. *Frontiers in Neuroscience*, (8 JUL). https://doi.org/10.3389/fnins.2014.00199

Plourde, G., Stapells, D. R., & Picton, T. W. (1991). The human auditory steady-state evoked potentials. *Acta Oto-Laryngologica*, *111*(S491), 153–160. https://doi.org/10.3109/00016489109136793

Reyes, S. A., Lockwood, A. H., Salvi, R. J., Coad, M. Lou, Wack, D. S., & Burkard, R. F. (2005). Mapping the 40-Hz auditory steady-state response using current density reconstructions. *Hearing Research*, *204*(1–2), 1–15. https://doi.org/10.1016/j.heares.2004.11.016

Ross, B., Herdman, A. T., & Pantev, C. (2005). Right hemispheric laterality of human 40 Hz auditory steady-state responses. *Cerebral Cortex*, *15*(12), 2029–2039. https://doi.org/10.1093/cercor/bhi078

Scherg, M., & Von Cramon, D. (1986). Evoked dipole source potentials of the human auditory cortex. *Electroencephalography and Clinical Neurophysiology*, *65*(5), 344–360. https://doi.org/10.1016/0168-5597(86)90014-6

Semmes, J. (1968). Hemispheric specialization: A possible clue to mechanism. *Neuropsychologia* (Vol. 6). Pergamon Press. https://doi.org/10.1016/0028-3932(68)90035-3

Stapells, D. R. (2010). Frequency-specific ABR and ASSRs threshold assessment in young infants. *A sound foundation through early amplification: An international conference* (pp. 409–448). https://doi.org/D21-P-1-10

Tervaniemi, M., Medvedev, S. V., Alho, K., Pakhomov, S. V., Roudas, M. S., Van Zuijen, T. L., & Näätänen, R. (2000). Lateralized automatic auditory processing of phonetic versus musical information: A PET study. *Human Brain Mapping*, *10*(2), 74–79. https://doi.org/10.1002/(SICI)1097-0193(200006)10:2<74::AID-HBM30>3.0.CO;2-2

Tiihonen, J., Hari, R., Kaukoranta, E., & Kajola, M. (1989). Interaural interaction in the human auditory cortex. *Audiology Official Organ of the International Society of Audiology*, *28*(1), 37–48.

Toga, A. W., & Thompson, P. M. (2003). Mapping brain asymmetry. *Nat Rev Neurosci*, *4*(1), 37–48. https://doi.org/10.1038/nrn1009

Wang, L., Uhrig, L., Jarraya, B., & Dehaene, S. (2015). Representation of Numerical and Sequential Patterns in Macaque and Human Brains. *Current Biology*, *25*(15), 1966–1974. https://doi.org/10.1016/j.cub.2015.06.035

583 Zatorre, R J, & Belin, P. (2001). Spectral and temporal processing in human auditory cortex.
584 Cerebral Cortex (New York, N.Y. : 1991), 11(10), 946–953.
585 https://doi.org/10.1093/cercor/11.10.946
586 Zatorre, Robert J, & Gandour, J. T. (2008). Neural specializations for speech and pitch: Moving
587 beyond the dichotomies. *Philosophical Transactions of the Royal Society B: Biological*
588 *Sciences*. https://doi.org/10.1098/rstb.2007.2161
589
590

Figure and table legends

Figure 1: Stimuli: (A) Amplitude-modulated pure tone (1000 Hz frequency), of 25ms duration with 5ms rise/fall time, presented 40 times in a second during 1s ON block interspersed by two OFF blocks (silent periods). **(B) Auditory stimulation conditions**: monaural left, monaural right and binaural.

Figure 2: (A) Group-level power spectrum averaged over all sensors, measured for monaural left (magenta), monaural right (green), binaural stimuli (blue), and baseline (black) conditions. **(B)** Spectral difference: Topographical distribution of induced 40 Hz spectral power during presentation of periodic auditory stimuli at 40 Hz for 1.) monaural left (left panel), 2.) monaural right (middle panel) and 3.) binaural condition (right panel). '*' mark the position of significant channels.

Figure 3: Sources of 40 Hz ASSRs for 1.) monaural left (1^{st} row), 2.) monaural right (2^{nd} row) and 3.) binaural conditions (3^{rd} row) represented from axial (1^{st} column), left (2^{nd} column) and right(3^{rd} column) view.

Figure 4: Large-scale neural model to mechanistically explain ASSR lateralization A.) Pipeline to calculate LI from empirical and simulated data. B.) Bar plots of group-level mean hemispheric laterality indices (LI) for 40 Hz spectral power obtained from reconstructed source (Empirical) and output of neural dynamics model simulation (Theoretical), C.) Variation of LI under parametric variation of global coupling(k) and mean delay (τ) in the large-scale neural model.

614

615 **Table 1:** t-statistic and *p* values of significant 40 Hz ASSRs clusters over scalp.

616

617 **Table 2:** List of 40 Hz ASSRs source labels with number of voxel activated in left and right

618 hemisphere.

Figure 1

(A)

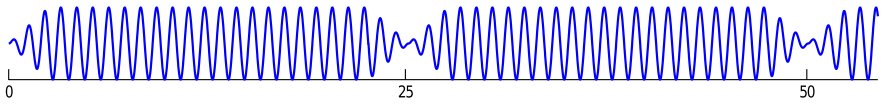

(B)

Figure 2

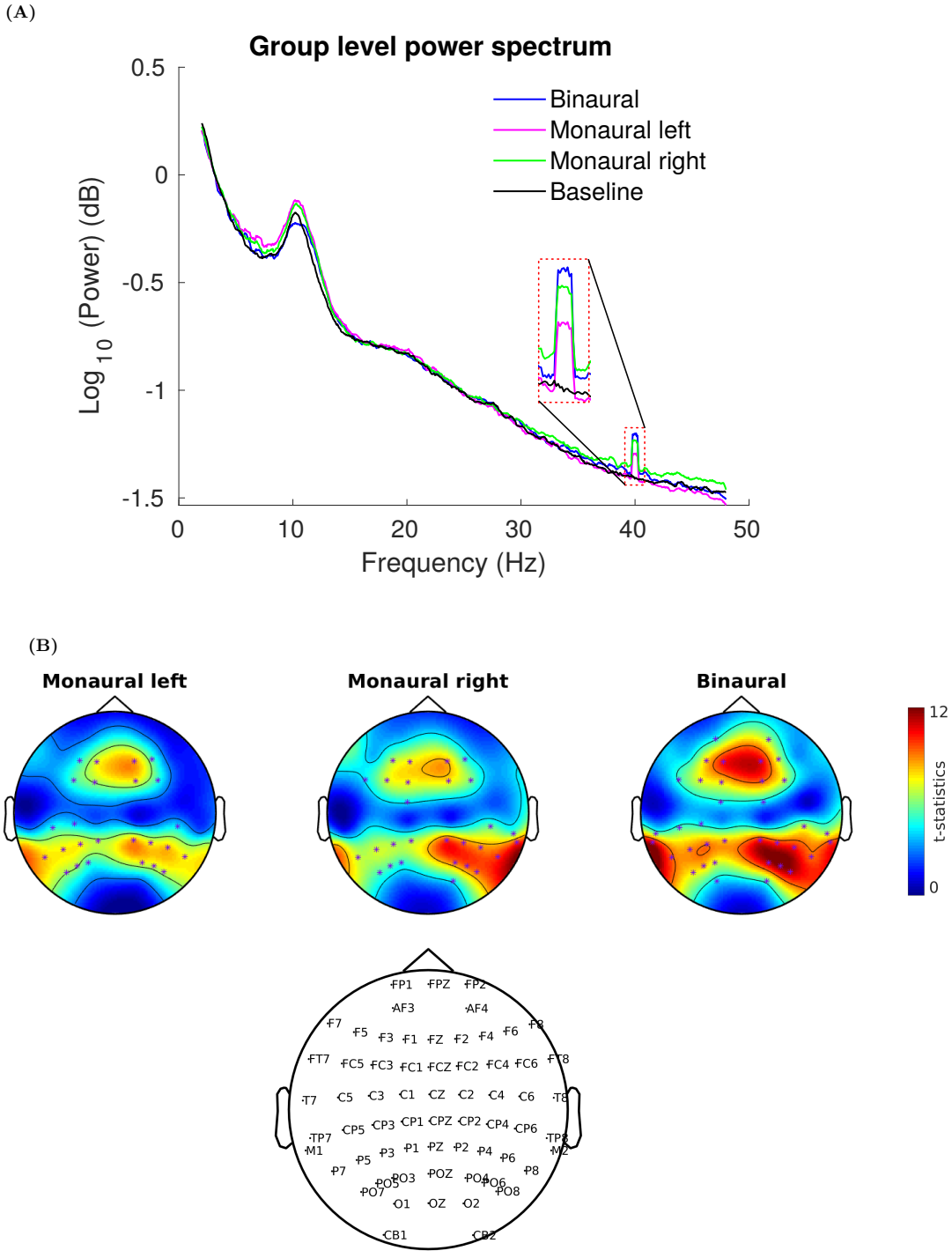

Figure 3

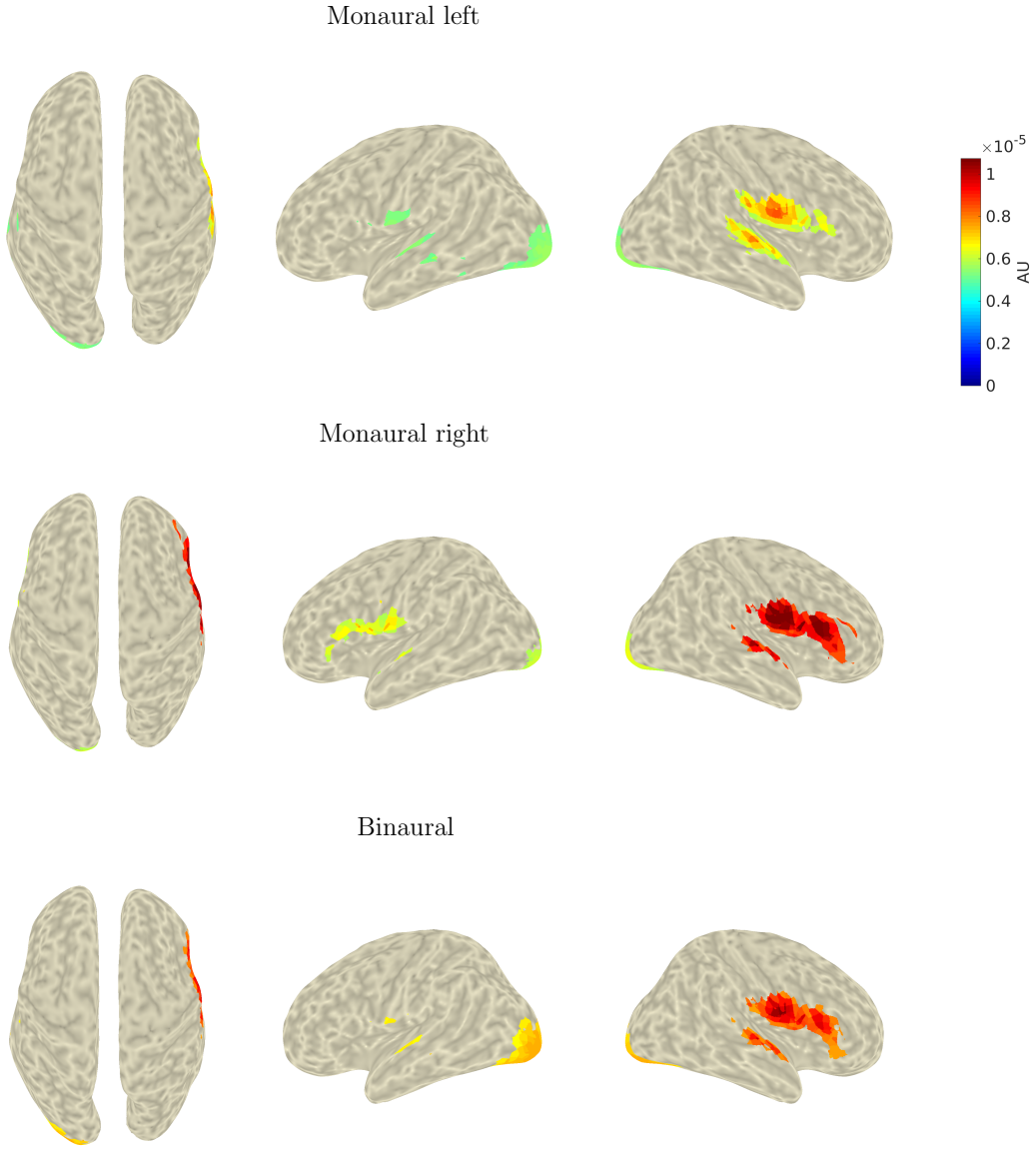

Figure 4

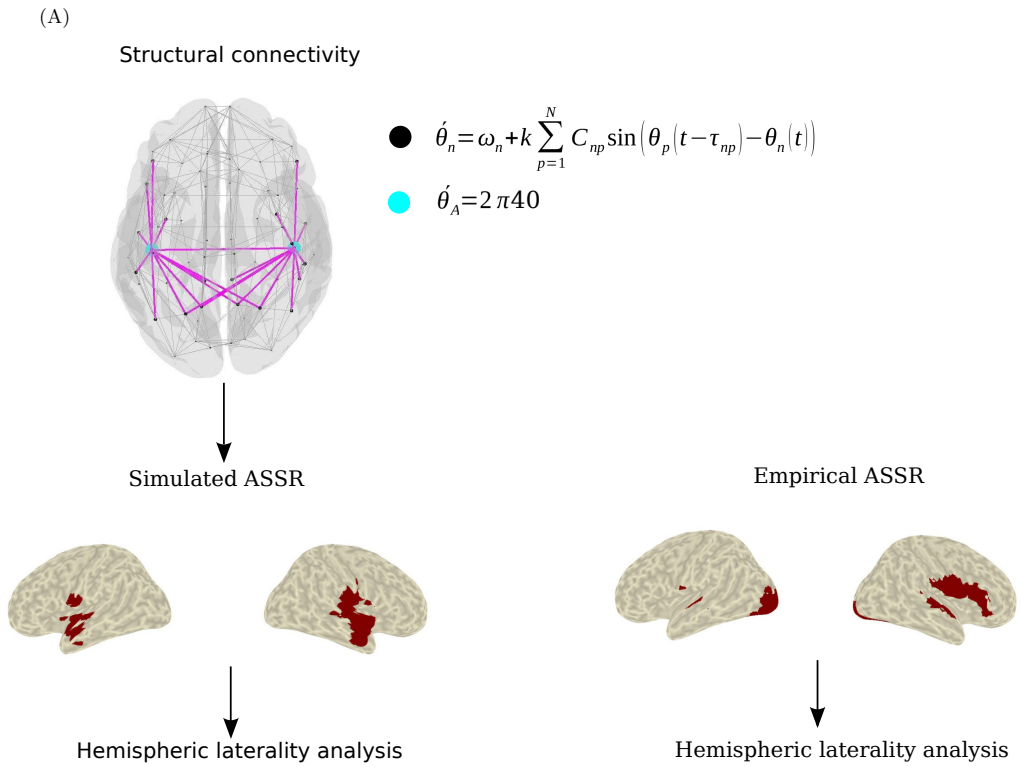

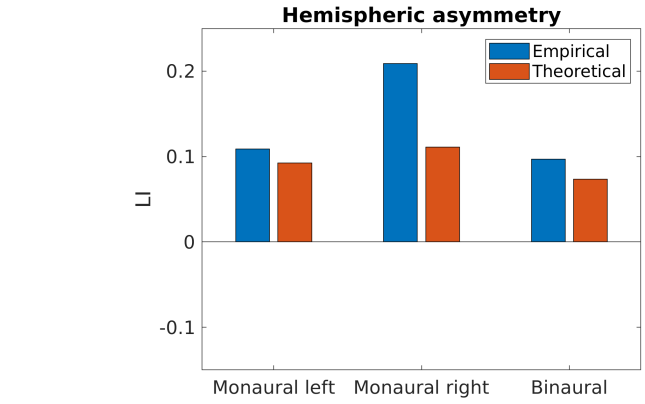

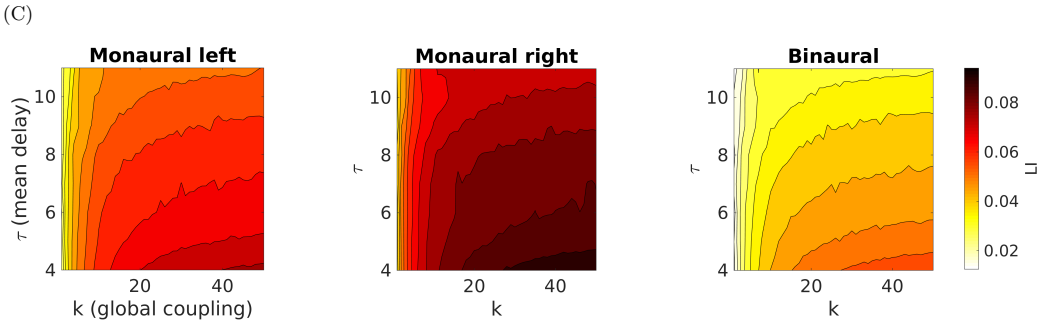

Table 1

	Monaural left		**Monaural right**		**Binaural**	
	t-score ($t_{(185)}$)	*p*-value	t-score ($t_{(185)}$)	*p*-value	t-score ($t_{(185)}$)	*p*-value
Fronto-central	119.67	< 0.001	146.64	< 0.001	214.80	< 0.001
Posterior region	69.45	< 0.001	83.94	< 0.001	116.90	< 0.001

Table 2

Monaural left			
Left hemisphere	No. of voxels	Right hemisphere	No. of voxels
Superior temporal	9	Superior temporal	24
Postcentral	3	Postcentral	14
Precentral	4	Precentral	12
Supramarginal	1	Supramarginal	10
Middle temporal lobe	3	Middle temporal lobe	1
Lateral occipital lobe	32	Pars Triangularis	2
Lingual	7	Pars Percularis	8
Fusiform	5	Transverse temporal	2
Pericalcarine	3		
Inferior temporal lobe	1		

Monaural right			
Precentral	13	Precentral	15
Pars Percularis	9	Pars Percularis	13
Pars Triangularis	5	Pars Triangularis	13
Postcentral	4	Postcentral	13
Superior temporal	6	Superior temporal	12
Lateral occipital lobe	19	Rostral middle frontal	3
Lingual	7	Pars Orbitalis	2
Cuneus	2	Supramarginal	2
Pericalcarine	2		
Fusiform	1		

Binaural			
Superior temporal	5	Superior temporal	17
Precentral	1	Precentral	15
Postcentral	1	Postcentral	13
Lateral occipital lobe	35	Pars Percularis	13
Lingual	14	Pars Triangularis	10
Fusiform	7	Supramarginal	3
Pericalcarine	4	Pars Orbitalis	2
Middle temporal lobe	1		